

Influence of chemical weathering and aging of iron oxides on the potential iron solubility of Saharan dust during simulated atmospheric processing

Zongbo Shi,¹ Michael D. Krom,¹ Steve Bonneville,¹ Alex R. Baker,² Charlie Bristow,³ Nick Drake,⁴ Graham Mann,⁵ Ken Carslaw,⁵ James B. McQuaid,⁵ Tim Jickells,² and Liane G. Benning¹

Received 1 April 2010; revised 14 September 2010; accepted 15 February 2011; published 21 May 2011.

[1] The flux of bioavailable Fe from mineral dust to the surface ocean is controlled not only by the processes in the atmosphere but also by the nature and source of the dust. In this study, we investigated how the nature of Fe minerals in the dust affects its potential Fe solubility (Fe_{psol}) employing traditional and modern geochemical, mineralogical, and microscopic techniques. The chemical and mineralogical compositions, particularly Fe mineralogy, in soil samples as dust precursors collected from North African dust source regions were determined. The Fe_{psol} was measured after 3 days of contact with sulfuric acid at pH 2 to simulate acid processes in the atmosphere. Fe_{psol} of the soil dust samples were compared with calculated predictions of Fe_{psol} based on the amount of individual Fe-bearing minerals present in the samples and Fe solubilities of corresponding standard minerals. The calculated Fe_{psol} deviated significantly from the measured Fe_{psol} of the soil dust samples. We attributed this to the variability in properties of Fe minerals (e.g., size of Fe oxides and heterogeneity of chemical compositions of clay minerals) in soil dusts in comparison to the standard minerals. There were, however, clear relationships between the degree of chemical weathering of North African soils and Fe_{psol} . The Parker index and ratio of ascorbate plus dithionite Fe to total Fe ((FeA+FeD)/FeT) are positively and negatively correlated with Fe_{psol} , respectively. In addition, the ratio of FeA/(FeA+FeD), which decreases with aging of the Fe oxides, was found to be positively correlated with Fe_{psol} in the soil dusts. Overall, our results indicate that there is a significant regional variability in the chemical and Fe mineralogical compositions of dusts across North African sources, as a result of the differences in chemical weathering and aging of Fe oxides. Furthermore, the indices for these weathering processes can provide an estimate of the fraction of Fe which can be solubilized if acid processed in the atmosphere.

Citation: Shi, Z., et al. (2011), Influence of chemical weathering and aging of iron oxides on the potential iron solubility of Saharan dust during simulated atmospheric processing, *Global Biogeochem. Cycles*, 25, GB2010, doi:10.1029/2010GB003837.

1. Introduction

[2] Iron (Fe) is an important micronutrient which can limit phytoplankton growth in the ocean [Boyd *et al.*, 2007]. While Fe supplied by dust is globally a rather small fraction of the total Fe inputs to the oceans, it is disproportionately important

in open ocean waters [Jickells *et al.*, 2005]. Bioavailable Fe supply can regulate and at times limit the primary productivity in large areas of the open oceans. Even in regions where phytoplankton growth is not Fe limited, such as the subtropical North Atlantic, dust input may affect primary productivity by stimulating nitrogen fixation [Mills *et al.*, 2004; Moore *et al.*, 2009]. As a result, the supply of bioavailable Fe from mineral dust can influence the CO₂ uptake from the atmosphere and affect Earth's climate [Jickells *et al.*, 2005]. The effect of aerosol Fe supply to the ocean on primary productivity and climate depends on the flux of bioavailable Fe, which is in turn partly controlled by the Fe solubility in the dust. Fe solubility in the dust however is one of the most uncertain parameters in current biogeochemical and earth system models.

[3] Available data indicate that apparent Fe solubility is higher in dust collected over the remote marine atmosphere

¹Earth and Biosphere Institute, School of Earth and Environment, University of Leeds, Leeds, UK.

²School of Environmental Sciences, University of East Anglia, Norwich, UK.

³Department of Earth and Planetary Sciences, Birkbeck College, University of London, London, UK.

⁴Department of Geography, King's College London, London, UK.

⁵Institute of Climate and Atmospheric Sciences, School of Earth and Environment, University of Leeds, Leeds, UK.

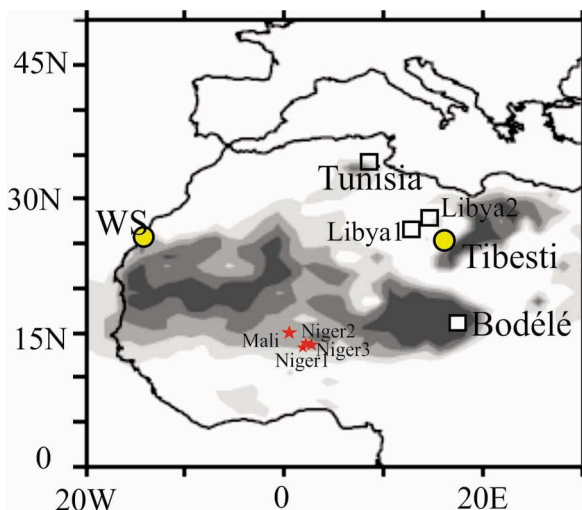


Figure 1. Locations of sampling sites. GPS coordinate of each sample are listed in Table 1. Spheres represent the samples from main Sahara Desert, stars represent the Sahel samples, and squares represent the paleolake samples. The contours represent the frequency of dust events (days per month when the Absorbing Aerosol Index equals or exceeds 1.0) in the African dust belt in 1987 [Prospero et al., 2002, Figure 3].

than in dust collected close to source areas [Hand et al., 2004; Baker et al., 2006]. This suggests that atmospheric processing can increase the solubility of Fe during dust transport [Mahowald et al., 2005; Baker and Croot, 2010]. One of the potentially important processes is the mobilization of Fe in acidic aerosol water which can reach pH values below 1–2 [Zhu et al., 1992; Keene et al., 2002; Meskhidze et al., 2003]. The dissolution and solubility of Fe in natural soil samples as dust precursors is strongly pH-dependent, with acidic pH triggering faster dissolution and increasing the fraction of total Fe that is dissolved [e.g., Cornell and Schwertmann, 2003; Desboeufs et al., 2005].

[4] The flux of bioavailable Fe to the surface ocean is controlled not only by the processes in the atmosphere which change its chemical and physical nature [e.g., Shi et al., 2009] but also by the nature of the mineral dust suspended in the source area. Mineral dust typically contains a mixture of several Fe-bearing minerals including: ferrihydrite and poorly crystalline Fe [Shi et al., 2009], hematite (Fe_2O_3) and goethite (FeOOH) [Arimoto et al., 2002; Lafon et al., 2004, 2006; Shen et al., 2006; Formenti et al., 2008; Shi et al., 2009], magnetite [Lazaro et al., 2008], and clay minerals such as illite, kaolinite, mixed layer illite/smectite, and smectite [Avila et al., 1997; Shi et al., 2005]. Jounet et al. [2008] measured the apparent Fe solubility of common Fe-bearing minerals including hematite, goethite, and clay minerals (e.g., illite and smectite) at atmospheric relevant pH conditions. They showed that the apparent Fe solubility of clay minerals is higher than that of Fe oxides (hematite and goethite). As a result they argued that it is the clay minerals alone that control the apparent Fe solubility in the dust. Schroth et al. [2009] showed that Fe solubility in Saharan dust was far lower than that measured in other sources of Fe

to the ocean. They suggested, based on X-ray absorption spectroscopy (XAS), that the presence of Fe as oxides, was responsible for the low Fe solubility in a Saharan dust. However, they identified these Fe oxides as mainly ferrihydrite which is generally considered to be highly soluble at the low pH [Schwertmann, 1991]. Shi et al. [2009] showed that Fe oxides (goethite and hematite) can be converted to labile Fe-rich nanoparticles by atmospheric processing. In their study, Fe nanoparticles were also shown to be present both in soils which had been through laboratory simulations of atmospheric processing and in natural dust samples from the western Mediterranean which had been cloud processed. Mackie et al. [2005] found that Fe was significantly mobilized below a threshold of pH 3.6, and between this threshold and pH 7.1, dissolved Fe falls to a minimum. Cwiertny et al. [2008a] found that the apparent Fe solubility is not correlated to the total Fe (FeT) or the surface area of the dust source materials. Fu et al. [2010] suggested that the apparent Fe solubility is dependent on pH, light, O_2 , type of acids (e.g., HCl, H_2SO_4 , HNO_3). Thus the complexity of the Fe solubility in mineral dust is only starting to be investigated and no patterns which can predict its general behavior have yet been found.

[5] In order to simulate the flux of bioavailable Fe to the ocean, a few models have been developed to understand how atmospheric processing may increase the apparent Fe solubility in the dust [e.g., Hand et al., 2004; Meskhidze et al., 2005; Luo et al., 2005; Fan et al., 2006; Solmon et al., 2009; Ito and Feng, 2010]. These models are able to capture the observed increase in apparent Fe solubility with distance from dust source regions. However, these models have not tried to include how processes in the source region might affect the ability of Fe in the mineral dust to be solubilized by atmospheric processes. In addition, these modeling studies have assumed hematite to be the only Fe-bearing mineral present in the dust. This simplifying assumption is questionable as it overlooks the wide range of potentially reactive Fe-bearing mineral which are known to be present in desert dusts.

[6] The aim of this study is to understand better how weathering processes in the source area can modify the Fe mineralogy of Saharan dust and hence affect the solubility of Fe when that dust is subjected to acidic atmospheric processing. Initially, the chemistry and mineralogy of soil samples used as surrogates for dust aerosol, collected from a series of known dust source regions in Africa was characterized. Laboratory experiments that simulated atmospheric processing on these samples and on reference minerals were carried out and Fe solubilities in these samples were determined. The measured Fe solubilities were then compared with calculated solubilities predicted from the contents of individual minerals and the solubilities of corresponding reference minerals and the results are discussed. Finally, we tried to link the chemical weathering processes in the dust source region with the potential of Fe to be dissolved in mineral dust during simulated atmospheric processing by acids.

2. Materials and Methodology

2.1. Samples

[7] Figure 1 shows the sample locations and Table 1 lists the relevant sample details. Soil samples were collected

Table 1. Locations and Properties of Soil Samples

	Origin	Class	BET Surface area (m ² g ⁻¹)
Tibesti	Tibesti Mountains, Libya, N25°35', E16°31'	Saharan, dried water course	11.83
WS	Western Saharan	Saharan, open desert	11.37
Niger1	Banizoumbou, Niger, N13°52', E2°62'	Sahel, open desert	14.25
Niger2	Gourou Goussou, Niger, N13°50' E2°23'	Sahel, open desert	33.78
Niger3	Giraffe Reserve, Koure, Niger N13°18', E2°34'	Sahel, open desert	11.2
Mali	Agoufou, Hombori, Mali, N15°22' W1°28'	Sahel, ephemeral lake	28.34
Bodele	Bodele Depression, Chad, N16°41' E17°47'	Paleolake	8.66
Tunisia	Chott el Djerid, Tunisia	Paleolake	11.35
Libya1	Wadi al Hyatt, Libya	Paleolake	4.75
Libya2	Wadi Ash Shatti, Libya	Paleolake	31.5

from major sources of present-day Saharan dust (Tibesti, western Sahara (WS), Bodélé and Tunisia), past major dust sources (Libya 1 and 2) and potential dust sources (Mali and Niger 1–3) [Brooks and Legrand, 2000; Prospero *et al.*, 2002; Drake *et al.*, 2008; Washington *et al.*, 2009; Bristow *et al.*, 2009]. As dried-up water courses, ephemeral dried lakes and paleolakes are known to be the major sources of atmospheric dusts [Teegen *et al.*, 2002; Prospero *et al.*, 2002], we targeted those areas for sampling. Further details about the samples used are given in the supplementary material (Text S1).¹

[8] All soil samples were dry sieved to <63 μm and then wet-sieved to less than 20 μm , freeze-dried and then disaggregated by gentle crushing. Minimum amounts of MQ water was used for sieving and that water was included in the freeze drying process. The dissolution of Fe from large particles should be minimal because the contact time of water with 20–63 μm soils was less than 5 min and we sieved the soils with MQ water. These <20 μm soil samples were used as surrogates for mineral dust as had been done previously [Lafon *et al.*, 2006]. In order to carry out the various geochemical and mineralogical analyses in this study, a relatively large quantity of sample was required. Lafon *et al.* [2006] showed that Fe speciation in Saharan soils was dependant on grain size but found that the geochemical properties of the <20 μm samples was similar to PM₁₀ (particulate matter less than 10 μm) samples obtained from a wind tunnel.

[9] In addition, we purchased standard clay minerals including illite, illite/smectite mixed layer (I/S), smectite and kaolinite (Table S1 in Text S1) from the clay mineral depository (<http://www.clays.org/SOURCE%20CLAYS/SCavailable.html>).

[10] Microgoethite and microhematite were synthesized in the laboratory according to Cornell and Schwertmann [2003]. Nanoematite was purchased from Scholz and Co. Ltd. and nanogoethite was made according to Cwiertny *et al.* [2008b]. Most particles in the nanogoethite sample were nanorod goethite (generally less than 100 nm) although a few ~100 nm hematite were also identified. However, the minor contamination of goethite by hematite did not affect our results because the purpose of that part of the study was to compare the solubilities of crystalline Fe oxides (not goethite or hematite individually) against size (see sections 4.1 and 4.2). Details of standard Fe oxides were shown in Table S1 in Text S1.

¹Auxiliary materials are available in the HTML. doi:10.1029/2010GB003837.

[11] Finally, a sample of ultrafine Arizona Test Dust (ATD, Power Technology Inc.) was used as an internal standard material to determine the precision of the sequential Fe extraction method (see below).

2.2. Simulated Atmospheric Processing

[12] About 15 mg of sieved soil dust sample or clay standard, or 2 mg of synthetic goethite or hematite were added to 500 mL Milli-Q water (~pH 5.3). Multiple cycling (3 times) between acidic (pH 2, 24 h) and circumneutral pH (pH 5–6, 24 h) were performed on the suspensions according to the procedure of Shi *et al.* [2009], Spokes *et al.* [1994] and Mackie *et al.* [2005]. H₂SO₄ was used instead of HNO₃ to avoid the oxidation of dissolved Fe(II) by NO₃⁻ [Cwiertny *et al.*, 2008a]. These pH cycles were intended to simulate the cycling of dust between atmospheric aerosols and clouds, which may happen during the transport of dust [Spokes *et al.*, 1994; Pruppacher and Jaenicke, 1995; Meskhidze *et al.*, 2003]. In the last low pH cycle, a 5 mL suspension sample was retrieved and filtered through a 0.2 μm pore size polycarbonate filter just before the pH was again raised to 5–6. Dissolved Fe concentration in the filtrate solution was measured using the ferrozine method after reduction by hydroxylamine hydrochloride solution [Viollier *et al.*, 2000]. Fe_s (mg dissolved Fe g⁻¹ sample) was defined as the dissolved Fe solubilized after 2 cycles between acid and circumneutral conditions plus a further 24 h at pH 2. The total time for the dust to be in contact with acid was 3 days. We used the term potentially Fe solubility (Fe_{psol}) defined as Fe_s/Fe_T × 100% to characterize and compare the solubilities of different samples of soils and minerals as a result of simulated atmospheric processing.

2.3. X-Ray Fluorescence Analysis

[13] Major elements were determined by X-Ray Fluorescence Analysis (XRF) on fused glass beads prepared from ignited powder with a sample to flux ratio of 1:5, 80% Li metaborate: 20% Li tetraborate flux. Results were quoted as component oxide weight percent, recalculated to include loss on ignition (Table 2). Samples were analyzed at the University of Leicester, Department of Geology on a PANalytical Axios Advanced XRF spectrometer calibrated using international and internal standards to ensure accurate data and included a lake sediment standard (LKSD-1) which yields a total elemental recovery of 98% and accuracy for all elements of better than 10% except for P₂O₅ which was 16% compared to quoted reference values (Table 2 and Table S2 in Text S1).

Table 2. Chemical Composition, Chemical Index of Alteration, Parker Index, and Potential Fe Solubility (Fe_{psol}) of Soil Samples (<20 μm)^a

Sample	SiO ₂	TiO ₂	Al ₂ O ₃	Fe ₂ O ₃	MnO	MgO	CaO	Na ₂ O	K ₂ O	P ₂ O ₅	SO ₃	LOI	Total	Si/Al	Fe/Al	Ca/Al	CIA	Parker	Fe _{psol} , %
Tibesti	48.74	0.94	17.66	6.88	0.10	3.70	5.91	0.69	2.21	0.21	0.29	11.70	99.02	2.43	0.58	0.51	80	117	5.6
WS	49.65	0.87	16.25	6.66	0.09	3.94	7.23	0.67	2.70	0.19	0.02	11.64	99.93	2.69	0.61	0.68	76	133	5.1
Niger1	51.69	2.01	19.11	8.29	0.13	0.64	0.67	0.05	1.13	0.14	0.04	14.77	98.64	2.38	0.65	0.05	93	34	1.0
Niger2	45.81	1.69	25.99	12.12	0.04	0.15	0.10	0.01	0.33	0.11	0.03	12.59	98.98	1.55	0.70	0.01	98	9	0.7
Niger3	72.32	2.04	12.69	3.86	0.05	0.39	0.30	0.09	1.04	0.08	0.03	6.72	99.62	5.02	0.46	0.04	90	32	2.4
Mali	55.10	0.99	21.95	6.07	0.04	1.57	0.37	0.14	2.57	0.13	<0.005	9.76	98.70	2.21	0.41	0.03	87	70	10.1
Bodele	18.01	0.19	3.05	1.39	0.12	5.57	35.20	0.94	0.38	0.15	0.35	35.59	100.93	5.21	0.68	17.67	49	294	16.9
Tunisia	23.26	0.30	4.98	2.22	0.04	9.71	14.13	8.19	1.74	0.12	3.73	25.94	94.36	4.12	0.67	4.35	22	521	17.3
Libya1	5.01	0.14	1.90	0.80	0.02	2.94	45.41	2.04	0.21	0.07	0.34	42.53	101.42	2.32	0.63	36.54	17	416	10.1
Libya2	56.12	0.60	14.12	4.90	0.02	3.09	0.78	3.70	2.46	0.14	0.84	11.16	97.94	3.50	0.52	0.08	54	209	6.6
LKSD-1	40.1	0.5	7.8	4.1	0.1	3.7	10.8	2.0	1.1	0.2	-	29.9	96.6						

^aNote: LOI is loss on ignition. LKSD-1 is a lake sediment reference sample. See Table S2 in Text S1 for reference concentration of elements.

2.4. Chemical Weathering Indices

[14] Two weathering indices were calculated based on bulk chemical compositions of the samples. The Parker index [Parker, 1970] is calculated by

$$\text{Parker index} = \left(\frac{(Na)_a}{0.35} \right) + \left(\frac{(Mg)_a}{0.9} \right) + \left(\frac{(K)_a}{0.25} \right) + \left(\frac{(Ca)_a}{0.7} \right) \times 100 \quad (1)$$

where $(X)_a$ indicates the atomic proportion of a given element, defined as atomic percentage divided by atomic weight. This index is based on the proportions of alkali and alkaline earth metals (Na, K, Mg and Ca) present and on their bond strength with oxygen (0.35, 0.9, 0.25, and 0.7, respectively) to determine the weathering of a given soil. Here, we did not correct the halite and carbonate/gypsum-related Ca for calculating the Parker index. This, however, should have minimum effect on the calculation of the Parker indices for the Saharan and Sahelian samples (see Table 2).

[15] Chemical Index of Alteration (CIA) [Nesbitt and Young, 1982] is calculated by

$$CIA = \frac{Al_2O_3}{Al_2O_3 + CaO^* + Na_2O^* + K_2O} \times 100 \quad (2)$$

where Al_2O_3 , CaO^* , Na_2O^* and K_2O are in molar fractions. CaO^* represents the amount of CaO in the silicate fraction of the sample, and Al_2O_3 and K_2O were both determined by XRF (Table 2). The calculation of Na_2O^* from the silicate fraction was made by subtracting the Na associated with halite (measured after a 12 h extraction with 1 M acetic acid using ion chromatography) from the total Na_2O measured by XRF. We followed the procedure developed by McLennan [1993] assuming CaO^* to be equivalent to Na_2O^* .

2.5. X-Ray Diffraction Analysis

[16] A D/MAX-250 (Rigaku, Japan) XRD scanning with Cu $K\alpha$ radiation at 40 kV, 125 mA was used for mineralogical analysis. The scanning speed was $-3^\circ (2\theta) \text{ min}^{-1}$ and the step size was $0.01^\circ (2\theta)$. The specimen was placed on a small cuboid trough made of aluminum for X-Ray Diffraction (XRD) analysis. Mineral phases were identified by means of ICDD PDF2 (International Centre for Diffraction Data Powder Diffraction Files) database based on the

d-spacing values and diffraction peak intensity. Weight percentages of different phases in the samples were semi-quantified based on the Petroleum Industry Standard Methods of China (FY-T5263-1995).

2.6. Scanning and Transmission Electron Microscopy

[17] Powder or filter samples were suspended in ethanol, dispersed by ultrasonication, and deposited on Al-stubs for Scanning Electron Microscopy (SEM) analysis or on Cu-grids covered by standard holey carbon films for Transmission Electron Microscopy (TEM) analysis. Samples were imaged using a Jeol JXA 8100 Superprobe SEM after coating with 3 nm Au or C. The SEM was operated at an accelerating voltage of 20 kV with a beam current 40–100 nA. A FEI CM200 FEG-TEM equipped with an Oxford Instrument Ultrathin window ISIS Energy Dispersive X-ray (EDX) spectrometer was used for high-resolution imaging and to analyze the chemical composition of individual particles. The FEG-TEM was operated at 200 kV. Finally, using TEM, selected area electron diffraction (SAED) patterns were acquired of representative particles.

2.7. Sequential Fe Extraction

[18] pH 7.5 buffered ascorbate extractions were performed over a period of 24 h to leach the chemically highly reactive amorphous and nanoparticulate Fe (hereafter referred to as FeA) [Hyacinthe et al., 2006; Raiswell et al., 2008]. The ascorbate extractant consisted of a deoxygenated solution of 50 g L⁻¹ sodium citrate and 50 g L⁻¹ sodium bicarbonate to which 10 g L⁻¹ of ascorbic acid was added. About 15 mg of sample was mixed with 10 mL of the ascorbate solution, shaken for 24 h at room temperature and then filtered through a 0.2 μm pore size polycarbonate filter. After the ascorbate extraction, the particles collected on the filters were subsequently extracted for 2 h with citrate-buffered dithionite to dissolve crystalline Fe(III) oxides, mainly goethite and hematite (hereafter referred to as FeD). This extraction consisted of a solution of 50 g L⁻¹ sodium dithionite in 0.35 M acetic acid and 0.2 M sodium citrate, buffered at pH 4.8. In addition, sodium acetate extractions were performed over a period of 2 h to selectively leach the carbonate-associated Fe in the paleolake samples (Bodèlè, Tunisia, Libya1 and Libya2) at a dust/liquid ratio of $\sim 30 \text{ mg}/10 \text{ mL}$. The sodium acetate solution was made of 1 M sodium acetate, buffered at pH 4.5 [Poulton and Canfield, 2005].

Table 3. Semiquantitative Mineralogical Composition of <20 μm Soils^a

	Q	K-F	Pla	Cal	Mg-C	Dol	Hem	Halite	Gyp	Anh	Noncrystalline	I/S	I	K	C	Clay total
Tibesti	44	1	-	8	-	3	-	-	-	-	-	23	15	2	4	43
WS	49	19	13	9	-	-	-	-	-	-	-	6	2	2	-	10
Niger2	25	-	-	-	-	-	-	-	-	-	-	-	-	75	-	75
Mali	56	1	-	-	-	-	-	-	-	-	-	16	3	25	-	43
Bodélé	7	-	-	-	86	-	-	-	-	-	-	4	-	3	-	7
Tunisia	35	10	2	5	-	-	-	1	44	-	-	3	-	-	-	3
Libya1	6	-	-	88	-	-	-	4	-	-	-	-	-	2	-	2
Libya2	8	-	-	-	-	-	-	1	1	3	54	15	2	16	-	33

^aNote: Q, quartz; K-F, K feldspar; Pla, Plagioclase; Cal, calcite; Mg-C, Mg-calcite; Dol, dolomite; Hem, hematite; Gyp, gypsum; A, anhydrite; I/S, mixed layer illite/smectite; I, illite; K, kaolinite; C, chlorite.

[19] Dissolved Fe concentrations in the filtrates passing through 0.2 μm pore size membrane filters were determined using the ferrozine method [Viollier *et al.*, 2000]. The precision of the pH-buffered ascorbate and dithionite extractions were tested on nine ATD replicates and showed a relative standard error of 7.5% for FeA and 9.7% for FeD. The precision of the pH-buffered sodium acetate extraction tested on 6 reference samples demonstrated a relative standard error of 4.4%.

[20] FeT (total Fe) in all soil samples and the ATD was measured by XRF. FeT in standard clay minerals was provided by the supplier.

[21] We defined free Fe ratio [e.g., Lafon *et al.*, 2004] as

$$\text{Free Fe ratio} = \frac{\text{FeA} + \text{FeD}}{\text{FeT}} \quad (3)$$

3. Results

3.1. Properties of Soil Dust Samples and Their Potential Fe Solubility

3.1.1. Chemical Composition

[22] Table 2 shows the chemical compositions of different soil samples. Tibesti and WS had chemical compositions characteristic of a quartz/feldspar/clay dominated soil. By contrast, the paleolake samples (Tunisia, Libya 1, and Bodélé)

had CaO as a main component while Libya2 mainly consisted of SiO₂ probably due to opaline silica (diatoms). The Sahel samples (Niger1–3, Mali) had low CaO and relatively high Fe₂O₃.

3.1.2. Mineralogical Composition

[23] Table 3 shows the semiquantitative mineral composition of the samples. Tibesti and WS were dominated by quartz but the former contained more clay minerals whereas the latter contained more K-feldspar and plagioclase. Within the paleolake samples, Libya1 was dominated by calcite, Bodélé by Mg-calcite, while Tunisia contained more than 40% of gypsum. These samples all had less than 10% clay minerals. Libya2 was somewhat different from the other paleolake samples in that it contained larger amount of clay minerals and 54% of unidentifiable and possibly amorphous materials. Tunisia, Libya1, and Libya2 samples also contained small amounts of halite. Niger 2 and Mali samples from the Sahel region consisted mainly of quartz and clay minerals, particularly kaolinite.

3.1.3. Extractable Fe

[24] Figure 2 and Table S3 in Text S1 show the fractions of FeA, FeD and FeT in the different samples (see glossary of terms used). FeT ranged from 5.6 to 79.4 mg g⁻¹ in the soil samples with (1) Libya1 and Bodélé samples relatively low: 5.6 and 9.7 mg g⁻¹, respectively, and (2) Niger1 and Niger2 samples relatively high: 52.0 and 79.4 mg g⁻¹, respectively.

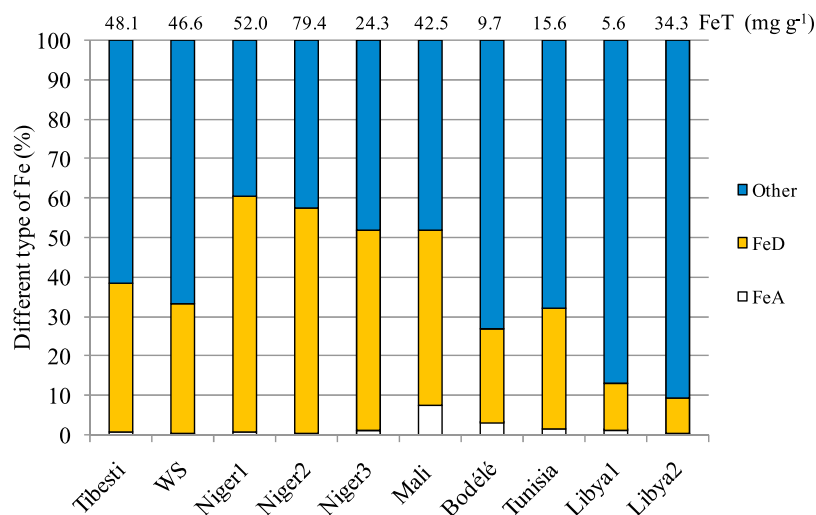


Figure 2. Percentages of ascorbate Fe (FeA), dithionite Fe (FeD), and other Fe to the total Fe (FeT) content. FeT of each sample (in mg g⁻¹) is shown above each column. The actual concentrations of different Fe species are given in Table S3 in Text S1.

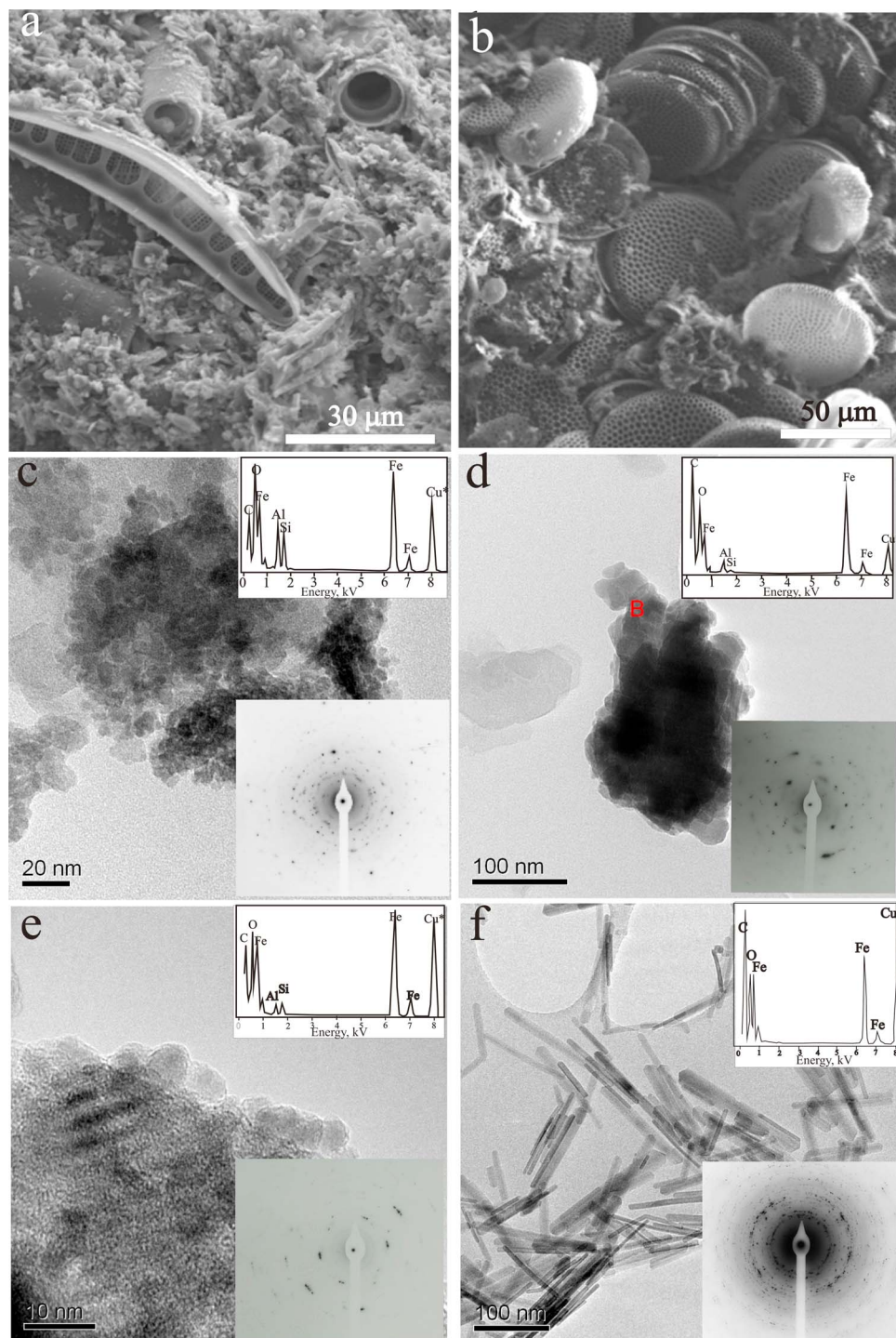


Figure 3. Microscopic properties of natural soil dust particles and laboratory-made nanogoethite particles. (a) SEM image of the Bodélé sample; (b) SEM image of the Libya2 sample; (c) TEM image, EDX spectrum, and SAED pattern of nanosized hematite particles in the Tibesti sample, identified by the *hkl* peaks (Miller indices, defining a specific plane where the diffraction occurs with specific d-spacing) 3.68, 2.70, 1.83, and 1.48 Å in SAED pattern; (d) TEM image, EDX spectrum, and SAED pattern of a goethite particle in Niger1 sample, identified by the *hkl* peaks 4.98, 4.18, 2.58, 2.45, and 1.72 Å in the SAED pattern; (e) TEM image, EDX spectrum, and SAED pattern of a poorly crystalline Fe oxide particle in the Niger1 sample; (f) TEM image, EDX spectrum, and SAED pattern of laboratory-made nanogoethite particles, identified by *hkl* peaks 4.18, 2.69, 2.25, 1.72, and 1.51 Å in the SAED pattern.

Generally, samples from the Bodélé and other paleolakes had lower FeT contents per mass of sample because of the “dilution effect” by authigenic minerals (calcite, gypsum and/or opaline silica).

[25] FeA varied from 0.08 (Libya1) to 3.10 mg g⁻¹ (Mali) (Table S3 in Text S1). In the Tibesti, WS, Niger1, Niger2, and Niger3 samples, FeA/FeT was typically less than 1.0%. In the paleolake samples (Bodélé, Tunisia, Libya1), FeA/FeT was generally higher than 1.0% although FeA/FeT in Libya2 was unusually low with only 0.4%. In the Mali sample, a location seasonally submerged under water, FeA/FeT reached a maximum at 7.3%.

[26] FeD ranged from 1.7 to 45.4 mg g⁻¹ and FeD/FeT varied from 9.0% to 59.6% in different soil samples (Table S3 in Text S1). FeD/FeT was particularly high in the Niger1, Niger2, and Niger3 samples (Figure 2). FeA+FeD represented the total Fe oxides, which accounted for 9.3 to 60.3% of the FeT in these samples (Figure 2 and Table S3 in Text S1).

[27] The remaining Fe represented the Fe in the aluminosilicate lattice and is often termed structural Fe [e.g., *Lafon et al.*, 2006]. Its content ranged from 39.7 to 90.7% in the soil samples (Figure 2).

[28] In addition, carbonate-associated Fe was measured in the paleolake samples, which accounted for 5.0%, 0.7%, 3.1%, and 0.1% of the FeT in the Bodélé, Tunisia, Libya1 and Libya2 samples, respectively.

3.1.4. Microscopic Properties of Fe-Rich Particles

[29] Figures 3a and 3b show the SEM images of two diatomite-containing paleolake samples (Bodélé and Libya2). The Bodélé sample contained diatoms that were cemented by authigenic carbonates (Figure 3a) which precipitated from the lake waters. The Libya2 sample was mainly composed of diatoms (Figure 3b) and their opaline silica composition agrees well with the XRD analysis showing the presence of large amounts of amorphous materials (Table 3), and the XRF data showing the large SiO₂ content (56%, Table 2).

[30] Figures 3c–3f show TEM images, EDX spectra, and SAED patterns of individual Fe-rich particles in Saharan soils, and an Fe oxide standard (nanogoethite). The EDX spectra shown in Figures 3c and 3d of Fe oxide particles exhibit some contributions of adjacent particles rich in Si and Al, however, typical d-spacings (see Figure 3 caption for details) allowed the identification of nanosized hematite (Figure 3c) and goethite (Figure 3d). In addition, some poorly crystalline Fe oxides were also identified (e.g., Figure 3e). In contrast, the synthetic Fe oxides showed characteristic well-crystalline morphologies and SAED pattern as exemplified by Figure 3f.

3.1.5. Potential Fe Solubility of the Soil Dust Samples

[31] Fe_{psol} of the soil samples ranged from 0.7% in Niger2 to 17.3% in Tunisia (Table 2). The two Niger samples (Niger 1–2), which had the highest FeT contents among all samples, showed the lowest Fe_{psol}. The highest Fe_{psol} were observed in the paleolake and lake samples (Bodélé, Tunisia, Libya1, and Mali), all of which were higher than 10%.

3.2. Properties of Standard Minerals and Their Potential Fe Solubility

3.2.1. Properties of Standard Minerals

[32] Major elemental compositions and extractable Fe for the standard clay minerals are presented in Tables S2 and S3,

respectively, in Text S1. FeT content ranged from 0.8 mg g⁻¹ in kaolinite to 55.5 mg g⁻¹ in illite. In addition to structural Fe (bound to silicate), XRD analysis detected the presence of Fe oxides in the I/S sample (further identified as goethite (FeG) by Direct Reflectance Spectrometry (DRS), see I/S sample in Table S3 in Text S1) and illite. However, the contribution of Fe oxide represented a small fraction of the FeT present in the standard clay minerals (Table S3 in Text S1). FeA, in the standard clay minerals (illite, I/S and smectite) were 0.9, 3.8, and 1.2% of FeT. Furthermore, FeA+FeD was less than 10% of FeT in the illite and smectite samples. As a comparison, in the microhematite, FeA was only 0.21 ± 0.01% while 99 ± 9% of the sample was measured as FeD (Table S3 in Text S1).

3.2.2. Potential Fe Solubility of Mineral Standards

[33] The soluble Fe (Fe_s) in the illite, I/S, smectite and kaolinite was 1.5, 0.3, 1.3 and 0.9 mg g⁻¹, respectively, while in the standard Fe oxides (Microhematite, nanohematite, microgoethite and nanogoethite), the Fe_s was greater at 2.7, 3.6, 6.7, 2.7 mg g⁻¹ (Figure S1 in Text S1). However, when expressed as Fe_{psol}, the values for standard clay minerals were considerably larger (2.7, 3.7, 5.2 and 13.4% in illite, I/S, smectite and kaolinite, respectively) than in the Fe oxides which ranged from 0.4% to 1.1% because the former contained far lower FeT. The Fe_{psol} in the nanosized hematite and goethite was higher than those in corresponding micro-sized minerals.

4. Discussion

[34] In this paper, we examined the factors controlling the solubility of Fe in North African soil dusts during simulated atmospheric processing. In the atmosphere, mineral aerosols age by taking up sulfate and/or nitrate [*Sullivan et al.*, 2007; *Shi et al.*, 2008]. The acid gases can be adsorbed onto mineral aerosol particles or scavenged by cloud droplets where the pH is usually above 3.0 [*Hegg et al.* 2002; *Straub et al.*, 2007]. As the cloud droplets evaporate, most of the water is lost, leading to an increase in the relative concentration of these dissolved acids and therefore the pH drops; these pH values can reach 1 or even lower [*Zhu et al.*, 1992; *Meskhidze et al.*, 2003]. Since Fe-rich dust particles tend to be smaller in size [i.e., *Cwiertyny et al.*, 2008a] and externally mixed with carbonate [i.e., *Sullivan et al.*, 2007; *Ito and Feng*, 2010], they are more likely to experience low pH conditions after long-range transport. Furthermore, since clouds commonly form and evaporate, this causes systematic fluctuations in mineral-aerosol water pH. Dust particles can be transported in the atmosphere for more than 2 weeks, therefore, they may encounter several cloud cycles during their lifetime [*Pruppacher and Jaenicke*, 1995; *Uno et al.*, 2009]. This complex atmospheric processing of Fe in the dust was illustrated by *Mackie et al.* [2005]. In order to simulate the pH fluctuations in the aerosol and cloud water, in this study we exposed soil samples to three acidic and two intermediate pH periods of 24 h each. We used the potential Fe solubility as a measure of the relative ability of simulated acidic processes to dissolve Fe in our samples. In the following sections, we attempt to predict Fe_{psol} of soil samples from the contents of different Fe-bearing minerals and solubilities of (Fe_s) of corresponding standard minerals, and then explain why

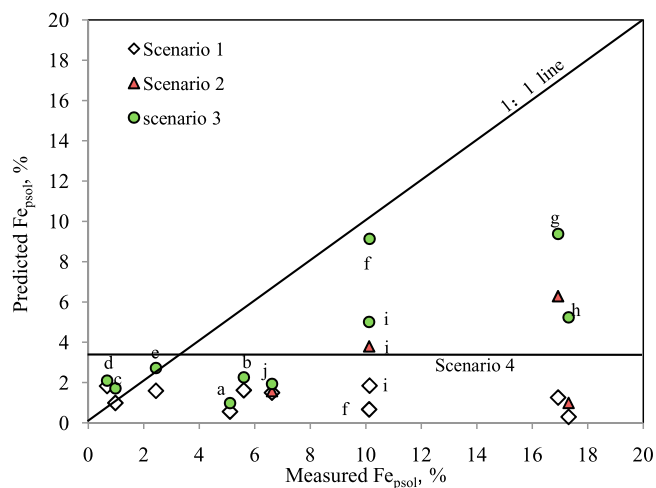


Figure 4. Measured versus predicted potential Fe solubility (Fe_{psol}) in North African soil dust samples. Predicted Fe_{psol} was calculated from contents of individual Fe minerals and measured Fe_{psol} of corresponding standard minerals. For a detailed explanation of scenario 1, 2, 3, and 4, see section 4.1. Scenario 4 created a straight line with predicted Fe solubility of about 3.5%. Because the amount of samples in Niger1 and Niger 3 was not enough for semiquantitative mineralogical analysis, we assumed total clay contents in these samples to be 30%. A 10% variation in the clay contents in these two samples leads to less than 30% changes in estimated Fe_{psol} . The sample numbers used are “a” Tibesti; “b” WS; “c” Niger1; “d” Niger2; “e” Niger3; “f” Mali; “g” Bodélé; “h” Tunisia; “i” Libya1; “j” Libya2.

this procedure does not seem able to predict Fe solubilities with acceptable accuracy. On this basis, we developed a new understanding of the critical factors that control the potential of Fe to be dissolved in the dust.

4.1. Predicting Potential Fe Solubility in Dust Samples

[35] Knowing the mineralogical contents of all our samples and the solubilities (Fe_s) of the corresponding standard Fe-bearing minerals (poorly crystalline Fe oxides, clay minerals, crystalline Fe oxides, calcite/dolomite/gypsum), we calculated the Fe_{psol} by summing soluble Fe from each Fe-bearing mineral.

$$PredictedFe_{psol} = \frac{\sum_i (Mass_i \times Fe_{s-i})}{FeT} \times 100 \quad (4)$$

where $Mass_i$ is the mass of Fe-bearing phase i (e.g., illite) (in g mineral g^{-1} sample); Fe_{s-i} is the Fe_s of the Fe-bearing phase i (mg g^{-1}); FeT is the total Fe content in a sample (mg g^{-1}). We applied four scenarios:

[36] Scenario 1. We assumed that total dissolved Fe came from crystalline Fe oxides and clay minerals only. For simplicity, Fe oxides and clay minerals were assumed to be present only as nanogoethite and illite in our sample. Note that the two selected phases exhibited the highest Fe_s among our set of standards (Figure S1 in Text S1). This scenario was similar to the methodology of *Journet et al.* [2008] to calculate the contribution of Fe oxides to total dissolved Fe pool in a model composite dust.

[37] Scenario 2. We assumed that Fe in calcite/dolomite (as Fe carbonate) was totally soluble during simulated atmospheric processing and that Fe in a gypsum standard was totally soluble (Fe content in the sample is $\sim 0.1\%$ [*Varjo et al.*, 2003]) as well. We only considered the paleolake samples because Fe carbonate (i.e., $FeCO_3$) can only be formed under anoxic conditions and the other samples do not contain gypsum. We calculated Fe_{psol} in the same manner as in scenario 1 but added the measured carbonate and gypsum-associated Fe for each paleolake sample (see section 2.7).

[38] Scenario 3. We made the same assumptions as in scenario 2 except that, in addition, we assumed that all the poorly crystalline or nanoparticulate Fe (FeA) was completely dissolved during the simulated atmospheric processing. Thus we calculated Fe_{psol} in the same manner as in scenario 2 but added the measured FeA for each sample. This scenario addressed the fact that ferrihydrite and amorphous Fe are very soluble at low pH [*Schwertmann*, 1991; *Shi et al.*, 2009].

[39] Scenario 4. We assumed that clay minerals were not contributing to Fe dissolution, that Fe oxides existed only as hematite (nanosized), and the Fe_s was 10 times bigger than the actually measured Fe_s (Table S3 in Text S1). This scenario was similar to that used by *Meskhidze et al.* [2005] and *Solmon et al.* [2009] in their atmospheric models.

[40] The results of these four calculation scenarios are plotted against our experimental data of Fe_{psol} in Figure 4. Overall, none of these above scenarios adequately predicted the variability of Fe_{psol} in dust precursors and, except for Niger1 and Niger2, these calculations significantly underestimated the measured Fe_{psol} . Indeed, the Root Mean Squares (RMS) of the four scenarios were very high (2.7, 2.2, 1.7 and 2.2 respectively), where RMS of an ideal fit is 0. These results suggest that the methodology of predicting Fe_{psol} from mineralogical compositions in a natural sample and Fe_s of standard mineral may not be applicable to real dust.

[41] In addition to the above calculations, we used a similar mineralogical distribution of Fe-bearing minerals in a composite dust as in the work of *Journet et al.* [2008], but our own Fe_{psol} measurements for the standard phases (determined after 3 d at pH 2) to predict the contribution of Fe oxides to the total soluble Fe. Assuming microhematite or microgoethite to be the only Fe oxide phase, the contribution of Fe oxides to total dissolved Fe was as high as 10% and this value increased to 21% if we assumed a smaller size for the Fe oxides (i.e., nanogoethite). The above mentioned discrepancies lead us to question the basic assumptions underlying our calculations, i.e., that standard Fe-bearing minerals are representative of the corresponding phases in natural dust samples.

4.2. Potential Fe Solubility of Clay Minerals and Fe Oxides in Natural Dusts

[42] The standard clay minerals used in this study (and other similar studies) were derived from natural sources (Table S1 in Text S1). Among them, the chemical and physical properties including their Fe contents vary dramatically (e.g., Table S2 in Text S1), even when the same type of clay mineral standard is concerned. For example, the illite sample used in the present study contained 22% and 66% more Fe than the two illite standards used by *Journet et al.* [2008]. This chemical heterogeneity is partly due to the differences in chemical weathering regimes and also the parent/

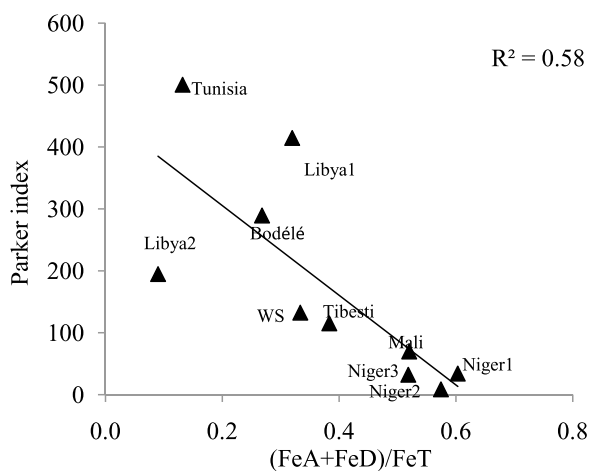


Figure 5. Plot of Parker weathering index against $(\text{FeA}+\text{FeD})/\text{FeT}$ (free Fe ratio) for soil dusts.

primary mineral from which the illite and generally other clay minerals originated [Meunier and Velde, 2004]. As a result of these heterogeneities, apparent Fe solubilities of the same type of standard clay mineral from different sources is likely to be different. For example, the two illite samples of Journet *et al.* [2008] exhibited apparent Fe solubility of 0.95% and 1.35%.

[43] In addition, once formed, clay minerals will undergo weathering processes, which affect the fate of the Fe species in them. It is well established that Fe can be solubilized from clay minerals to form Fe oxides in soils [McFadden and Hendricks, 1985], often as nanometer sized particles. XRD and DRS revealed the presence of Fe oxides (data not shown) in our standard illite and I/S samples. Therefore, assessing the Fe_{psol} of clay mineral standard is problematic as they often also contain Fe oxides that can dissolve with the clay mineral under acidic conditions.

[44] Furthermore, the choice of a single phase of pure Fe oxide synthesized in the laboratory to assess the Fe_{psol} of naturally occurring Fe oxides in mineral dust is also problematic. The differences in the formation conditions between the natural and laboratory settings in term of temperature, ionic strength, pH and chemical composition affect the mineralogy of Fe oxides formed as well as their physical and chemical properties. For instance, we found in our soil samples some Fe oxides that were poor in crystal order or even amorphous, often in the 5–10 nm size range (i.e., Figures 3c–3e) and therefore have a very large specific surface area. By contrast, our synthetic Fe oxides were well crystallized with characteristic morphologies and larger sizes (e.g., Figure 3f). These differences between natural and synthetic Fe oxides have been widely reported [Kampf and Schwertmann, 1983; Schwertmann and Latham, 1986; Anand and Gilkes, 1987; Fontes *et al.*, 1992; Costantini *et al.*, 2006]. Since the solubilities of Fe oxides and clay minerals are primarily controlled by specific surface area, grain size, purity and crystal order which are themselves highly sensitive to chemical and environmental conditions, it is not surprising that synthetic pure Fe oxides [Cornell and Schwertmann, 2003] and standard clay minerals [Meunier and Velde, 2004] do not reflect accurately the Fe solubility of the spectrum of Fe-bearing minerals potentially present in real mineral dust. Therefore the

assumption underlying our calculations that the standard Fe-bearing minerals are representative of the corresponding phases in all natural soil samples is unlikely to be valid. We suggest that this is the reason why we failed to predict the Fe_{psol} of our natural dust samples from the Fe_{s} of the standard Fe-bearing phases in them (scenario 1–3).

[45] For a similar reason, when using the characteristics of standard minerals to interpret and quantify the phases in complex natural samples, one should be cautious. For example, although we agree with Schroth *et al.* [2009] that Fe speciation of natural samples may control their apparent Fe solubility, these authors' interpretation that the dominant phase of Fe oxyhydroxides in Saharan dust is ferrihydrite (~70% of FeT) based on XAS identification is not in agreement with our data. We determined only 0.3–7.4% of our dust precursor samples to be ferrihydrite or amorphous Fe as extracted by ascorbate [Kostka and Luther, 1994; Hyacinthe *et al.*, 2006; Raiswell *et al.*, 2008] (Table S3 in Text S1). This has critical implications since ferrihydrite is orders of magnitude more soluble under simulated atmospheric processing than goethite and hematite [Schwertmann, 1991; Shi *et al.*, 2009]. None of our samples showed Fe_{psol} close to values of 70% which would be expected if 70% of the FeT was ferrihydrite. We consider it much more likely that crystalline Fe oxides (FeD) will dominate over ferrihydrite or poorly crystalline Fe in Sahara and Sahel soils (FeA; Figure 2) because ferrihydrite is only likely to be stable under most desert conditions for a relatively short time [Cornell and Schwertmann, 2003].

4.3. Dependence of Fe_{psol} on Degree of Chemical Weathering and Aging of Fe Oxides

[46] Since it was not possible to predict Fe_{psol} from the component minerals, we set out to determine if an understanding of the weathering processes in the source area might be used to develop a more accurate proxy for predicting the potential of Fe to dissolve during simulated atmospheric processing.

[47] In order to assess the degree of weathering of our dust source samples, we calculated three potentially relevant parameters: The Parker weathering index, the CIA, and the free Fe ratio $((\text{FeA}+\text{FeD})/\text{FeT})$; see equation (3)). The Parker weathering index is considered the most appropriate for application to weathering of heterogeneous parent rocks [Price and Velbel, 2003]. Unlike Price and Velbel [2003], we found that CIA was also a good index to represent the degree of weathering in our samples since it was highly correlated with the Parker index (Figure S2 in Text S1). The free Fe ratio has also been used as an indicator of soil maturity and degree of chemical weathering [e.g., Torrent *et al.*, 1980; Arduino *et al.*, 1984; Egli *et al.*, 2001]. The good correlations between the free Fe ratio, the CIA and, and the Parker index (Figure 5 and Figure S3 in Text S1) support our argument that the former is a good weathering index. This is consistent with our understanding of the sequence of chemical weathering of Fe-containing minerals particularly under desert conditions. As the parent rock weathers and soil develops, the original Fe-bearing minerals (including clay minerals) chemically weather releasing Fe which is subsequently converted into poorly crystalline Fe oxides (FeA). In turn, these labile Fe oxides are then aged and transformed into crystalline Fe oxides [McFadden and Hendricks, 1985; Leigh, 1996; Cornell

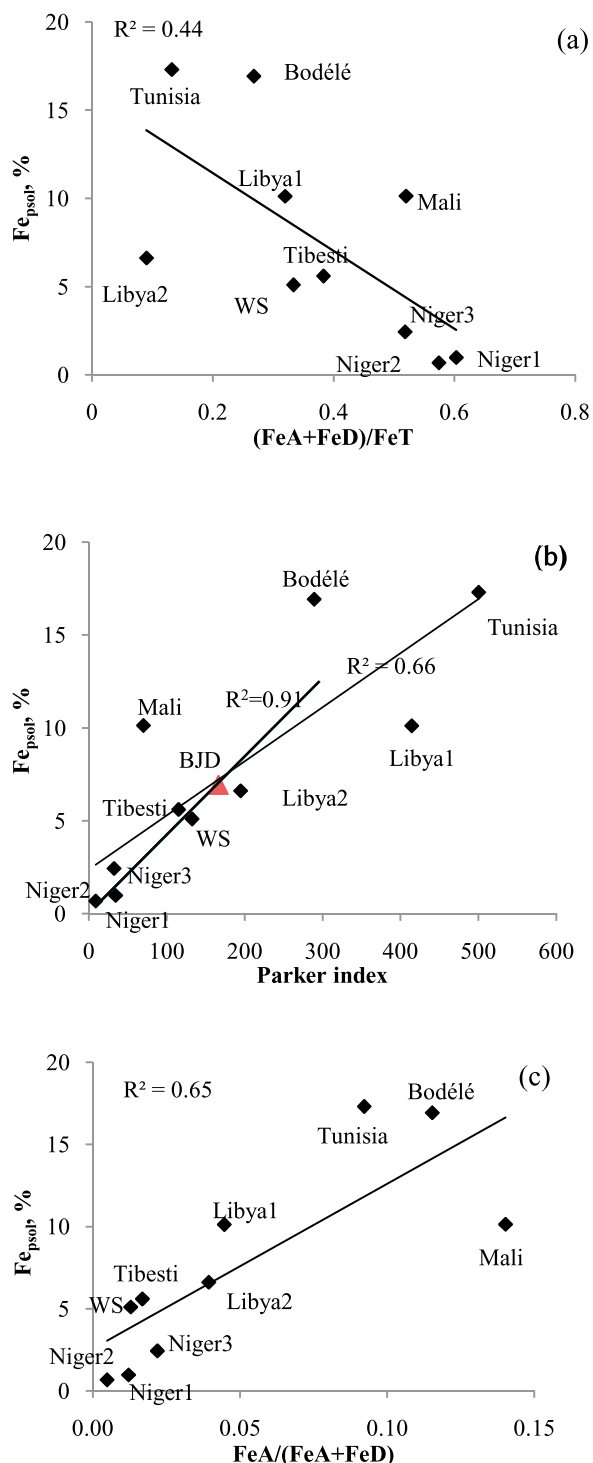


Figure 6. Correlation of potential Fe solubility (Fe_{psol}) with (a) $(FeA+FeD)/FeT$ (free Fe ratio); (b) Parker index; and (c) $FeA/(FeA+FeD)$ for soil dusts. The triangle data point (BJD) in Figure 6b was from an Asian dustfall collected in Beijing, China, after a super dust storm. This data point was not included in the calculation of regression line. The regression line with $r^2 = 0.66$ is based on all the data points, and the line with $r^2 = 0.91$ is based on samples excluding paleolake and lake deposit samples (see section 2.4).

and Schwertmann, 2003; Torrent *et al.*, 2007]. Initially, the minerals that are easiest to break down weather, and a relatively large amount of FeA forms. This FeA is converted over time to more refractory goethite and hematite (together measured as FeD). With time, the relative amount of FeA produced decreases and FeD increases. In the extreme case, which did not happen in our samples all the Fe in the rock/soil (FeT) is converted into FeD.

[48] In this study, the soils can be divided into 3 groups. The Sahel soils (Niger1, Niger2, Niger3 and Mali), which were subjected to high temperatures combined with relatively high rainfall, were the most intensively weathered with the highest free Fe ratio, the highest CIA (Table 2 and Figure S4 in Text S1) and the lowest Parker Index (Figure 5). The samples from Tibesti and western Sahara (samples: Tibesti and WS) have an intermediate degree of chemical weathering, while the samples from the dried-up paleolakes (Bodélé, Tunisia, Libya1 and Libya2) in the main Sahara Desert have a high Parker index, low CIA index and the lowest free Fe ratios. The free Fe ratio was 0.36 ± 0.04 from the Saharan region and 0.57 ± 0.04 from the Sahel region. Our results were comparable to the free Fe ratios reported previously for dust aerosols originating from the Saharan (0.35 ± 0.07) and Sahel (0.58 ± 0.03) regions (calculated from Table 1 in the work of Lazaro *et al.* [2008]). Lafon *et al.* [2004] also reported a lower free Fe ratio in the Saharan dust samples (0.44 ± 0.11) and higher free Fe ratio in the local Niger dust samples (0.65 ± 0.04). The high free Fe ratios in our Niger samples (Niger1–3) also compare well with those measured on ground-based dust aerosols collected at Banizoumbou [Formenti *et al.*, 2008]. Likewise, Moreno *et al.* [2006] reported a higher CIA in soils from the Sahel region than those from the Sahara.

[49] Having plotted Fe_{psol} against the different weathering indices (Figures 6a and 6b and Figure S4 in Text S1), we observed a clear relationship between the degree of chemical weathering determined by the three indices and the Fe_{psol} . The more chemically weathered the soil sample, the less Fe_{psol} was measured (Figures 6a and 6b and Figure S4 in Text S1).

[50] We also observed a systematic variation in the aging of Fe oxides as poorly crystalline Fe oxides, extracted by oxalate (FeO) or by ascorbate (FeA) [Reyes and Torrent, 1997], “age” and are converted into goethite and hematite measured as (FeD) in the dust source regions.

[51] $FeA/(FeA+FeD)$ or $FeO/(FeO+FeD)$ is widely used to characterize soil development [e.g., Thompson *et al.*, 2006; Lair *et al.*, 2009]. We observed a positive correlation ($r^2 = 0.65$) between $FeA/(FeA+FeD)$ and Fe_{psol} (Figure 6c) indicating that aging of Fe oxides may also affect Fe_{psol} . This is in agreement with our understanding that poorly crystalline and amorphous Fe have a higher Fe solubility [Schwertmann, 1991]. The highest $FeA/(FeA+FeD)$ ratios were found in samples from paleolakes which were less weathered, as indicated by both the CIA and Parker index (Figure 6c and Figure S2 in Text S1). The $FeA/(FeA+FeD)$ for the Bodélé sample was particularly high because labile Fe in minerals formed in the reducing conditions in the original paleolake Chad sediments, were buried with carbonate-diatomite (Figure 3a and Bristow *et al.* [2009]) and preserved in their original state until they were exposed and the solid was sand-blasted to form modern Saharan dust. By contrast, our Niger

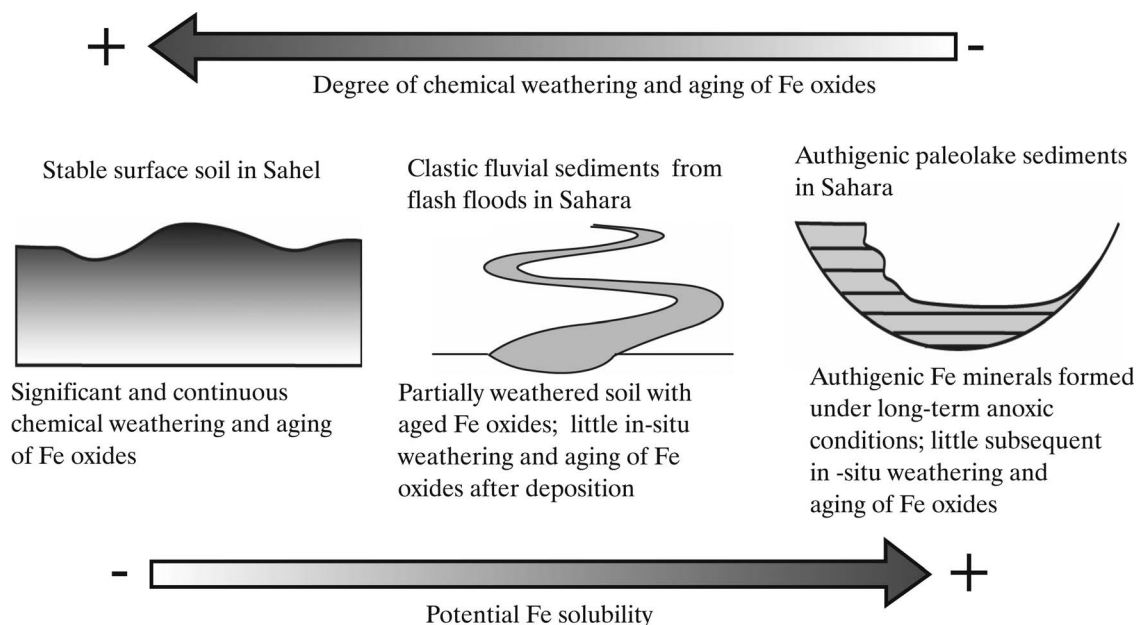


Figure 7. A conceptual model linking the regional variability in weathering and aging of Fe oxides and the potential Fe solubility in soil dusts. A higher degree of weathering (lower Parker index and higher free Fe ratio) and prolonged aging of Fe oxides (lower $\text{FeA}/(\text{FeA}+\text{FeD})$) lead to a lower potential Fe solubility.

(Sahel) samples have been subjected to relatively strong chemical weathering; the FeA content was the lowest among all our samples. We also found that the plot of the ratio of hematite to goethite Fe against Fe_{psol} shows an inverse correlation. This is consistent with the known conversion of goethite into more refractory hematite (Figure S5 in Text S1) as chemical weathering progresses [Cornell and Schwertmann, 2003].

[52] Thus our study shows a clear systematic pattern between regional characteristics of chemical weathering and aging of Fe oxides in the dust source areas and the potential for Fe to be dissolved in the soil dust samples subjected to simulated atmospheric processing. A conceptual model is proposed in Figure 7. In areas with stable soil surfaces and bedrock in the Sahel, the degree of weathering is very high (lower Parker index) and more crystalline Fe is present (lower $\text{FeA}/(\text{FeA}+\text{FeD})$) (e.g., Niger1, Niger2, and Niger3). This leads to a lower Fe_{psol} . In the authigenic lake sediments (e.g., Bodélé, Tunisia, Libya1 and Libya2), there is little chemical weathering and a larger amount of poorly crystalline Fe (FeA) and/or Fe carbonate is present because these authigenic minerals are well preserved in a carbonate/diatomite-rich deposits after formation in the anoxic conditions (e.g., Figures 3a and 3b). This leads to a high Fe_{psol} . In the clastic fluvial sediments from the flash floods in the Sahara (e.g., Tibesti), the degree of weathering and aging of Fe oxides are at an intermediate level, and therefore the Fe_{psol} is also intermediate.

[53] These results indicate that both the chemical weathering and aging of Fe oxides act as mechanisms to decrease the Fe_{psol} . This is further supported by the high correlation of Fe_{psol} with covariants like $\text{FeA}/(\text{FeA}+\text{FeD})$ and Parker index.

$$\text{Fe}_{\text{psol}} = 72.74 \times \text{FeA}/(\text{FeA} + \text{FeD}) + 0.021 \times \text{Parker} - 0.02$$

$$r^2 = 0.95 \quad (5)$$

When used to predict Fe_{psol} , the RMS error was 1.3 (free Fe ratio), 1.1 ($\text{FeA}/(\text{FeA}+\text{FeD})$), 1.1 (CIA) and 1.1 (Parker). These are much lower than the previously used methods to predict Fe_{psol} in soil dusts (see section 4.1). When using $\text{FeA}/(\text{FeA}+\text{FeD})$ and Parker index together to predict Fe_{psol} , the RMS error was 0.5, which is significantly lower than all other predictions.

4.4. Atmospheric Implications and Outlook

[54] It is important in climate models to be able to predict the Fe solubilities of mineral aerosols. Previously hematite has been used to predict apparent Fe solubilities in mineral aerosols [e.g., Hand et al., 2004; Meskhidze et al., 2005; Luo et al., 2005; Fan et al., 2006; Solmon et al., 2009; Ito and Feng, 2010]. We show here that using this simplified model could lead to a 5 times overestimation to a 5 times underestimation compared to the measured Fe_{psol} in real North African soil samples. Furthermore, we showed that the significant regional variability in the mineralogical compositions of the dust in North Africa, as a result of the differential chemical weathering and aging of Fe oxides in the source areas, is a critical factor controlling the potential Fe solubility in mineral dust. Therefore, this should be considered in future modeling studies to more accurately simulate the Fe solubilization in the dust during atmospheric processing.

[55] In order to provide an initial estimate of the potential of the Fe in a dust sample to be solubilized, we have developed two equations:

$$\text{Fe}_{\text{psol}} = -22.1 \times \text{free Fe ratio} + 15.8 \quad (6)$$

or

$$\text{Fe}_{\text{psol}} = 0.029 \times \text{Parker} + 2.38 \quad (7)$$

In these equations, we assumed that the dust sample has undergone acid processing at pH 2 for 3 days. The free Fe ratio is a parameter that has commonly been measured on mineral aerosols [Lafon *et al.*, 2004, 2006; Lazaro *et al.*, 2008; Formenti *et al.*, 2008], while the Parker Index can be calculated from bulk chemical composition of the samples using equation (1). As an independent test of our relationship, we plotted both Fe_{psol} and Parker index of an Asian dustfall sample collected after a major dust storm in Beijing [Shao *et al.*, 2008] on Figure 6b. The data point (triangle, BJD) fitted very closely on our regression line.

[56] We noted that our simulated atmospheric processing experiments are idealistic and do not take into account the complexity of Fe dissolution in the dust under actual atmospheric conditions or upon mixing with seawater [Baker and Croot, 2010]. Indeed, in addition to the nature of Fe in the dust proposed in this paper, several other parameters have to be predicted or measured before a model can accurately simulate the solubilization of Fe in dust during actual atmospheric processing. These include the pH (and buffer capacity) of the aerosol and the acid exposure time [i.e., Mackie *et al.*, 2005], or the heterogeneity of Fe-containing and Ca-containing dust particles and their affinity to different acidic gases [i.e., Sullivan *et al.*, 2007; Shi *et al.*, 2008]. Such models also need to take account of the presence and concentration of organic ligands, possible photoreduction [Siefert *et al.*, 1994; Cornell and Schwertmann, 2003; Fu *et al.*, 2010], and the kinetics of Fe dissolution at different atmospheric conditions.

[57] In summary, we have established in this paper that it is inappropriate to estimate the Fe solubility in a dust sample according to its content of Fe oxides and clay minerals and the solubilities of standard minerals; we showed that chemical weathering and Fe oxides aging processes in the dust source regions led to a significant regional variability in the chemical and mineralogical compositions of the dust samples in North Africa, which controlled the potential of Fe to be solubilized during simulated atmospheric processing.

Notation

- FeA poorly crystalline or nanoparticulate Fe, extractable by ascorbate solution (mg Fe g^{-1} sample).
- FeD oxide Fe, mainly goethite and hematite, extractable by citrate-buffered dithionite solution (mg Fe g^{-1} sample).
- FeT total Fe, determined by X-ray Fluorescence (mg Fe g^{-1} sample).
- Fe_s soluble Fe after simulated atmospheric processing (mg Fe g^{-1} sample).
- Fe_{psol} potential Fe solubility, equals to $Fe_s/FeT \times 100$.

[58] **Acknowledgments.** This work was supported by NERC (NE/E011470/1, PI: M. D. Krom). S. Bonneville and L. G. Benning thank NERC for financial support (NE/C004566/1; PI: L. G. Benning). C. Bristow thanks the Royal Geographical Society and the Gilchrist Educational Trust for supporting BoDEX and sample collection within the Bodélé Depression, Chad. Two anonymous reviewers are greatly thanked for their constructive and detailed review comments. Jose Torrent at Departamento de Ciencias y Recursos Agrícolas y Forestales Universidad de Córdoba, Spain, was acknowledged for his help in DRS analysis. N. Hanan from Colorado State University provided soil samples from Mali. J. Ratnam and B. Brooks from University of Leeds (UoL) helped to collect the Mali and Sahel samples. R. Mortimer, S. Shaw, H. P. Vu, A. Xylouri, L. Brinza, J. D. Rodriguez Blanco, and R. Raiswell at School of Earth and Environment and M. Ward,

R. Walshaw, and J. Harrington at LEMSC of UoL are acknowledged for their comments or technical help. L. Shao and W. Li at China University of Mining and Technology collected the Beijing dust sample. A. Nenes and P. Kumar from Georgia Institute of Technology are acknowledged for providing the kaolinite standard.

References

- Anand, R. R., and R. J. Gilkes (1987), Variations in the properties of iron oxides within individual specimens of lateritic duricrust, *Aust. J. Soil Res.*, *25*, 287–302, doi:10.1071/SR9870287.
- Arduino, E., E. Barberis, F. Carraro, and M. G. Forno (1984), Estimating relative ages from iron-oxide/total-iron ratios of soils in the western Po Valley, Italy, *Geoderma*, *33*, 39–52, doi:10.1016/0016-7061(84)90088-0.
- Arimoto, R., W. Balsam, and C. Schloesslin (2002), Visible spectroscopy of aerosol particles collected on filters: Iron-oxide minerals, *Atmos. Environ.*, *36*, 89–96, doi:10.1016/S1352-2310(01)00465-4.
- Avila, A., I. Queralt-Mitjans, and A. Alrcona (1997), Mineralogical composition of African dust delivered by red rains over northeastern Spain, *J. Geophys. Res.*, *102*(D18), 21,977–21,996, doi:10.1029/97JD00485.
- Baker, A. R., and P. L. Croot (2010), Atmospheric and marine controls on aerosol iron solubility in seawater, *Mar. Chem.*, *120*, 4–13, doi:10.1016/j.marchem.2008.09.003.
- Baker, A. R., T. D. Jickells, M. Witt, and K. L. Linge (2006), Trends in the solubility of iron, aluminium, manganese and phosphorus in aerosol collected over the Atlantic Ocean, *Mar. Chem.*, *98*, 43–58, doi:10.1016/j.marchem.2005.06.004.
- Boyd, P. W., et al. (2007), Mesoscale iron enrichment experiments 1993–2005: Synthesis and future directions, *Science*, *315*, 612–617, doi:10.1126/science.1131669.
- Bristow, C., N. A. Drake, and S. Armitage (2009), Deflation in the dustiest place on Earth: The Bodélé Depression, Chad, *Geomorphology*, *105*, 50–58, doi:10.1016/j.geomorph.2007.12.014.
- Brooks, N., and M. Legrand (2000), Dust variability over northern Africa and rainfall in the Sahel, in *Linking Climate Change to Land Surface Change*, edited by S. McLaren, pp. 1–26, D. Kniveton Kluwer Acad., Dordrecht.
- Cornell, R. M., and U. Schwertmann (2003), *The Iron Oxides: Structure, Properties, Reactions, Occurrence and Uses*, Wiley-VCH, New York.
- Costantini, E. A. C., S. Lessovaia, and Y. Vodyanitskii (2006), Using the analysis of iron and iron oxides in paleosols (TEM, geochemistry and iron forms) for the assessment of present and past pedogenesis, *Quat. Int.*, *156–157*, 200–211, doi:10.1016/j.quaint.2006.05.008.
- Cwiertny, D. M., J. Baltusaitis, G. J. Hunter, A. Laskin, M. M. Scherer, and V. H. Grassian (2008a), Characterization and acid-mobilization study of iron-containing mineral dust source materials, *J. Geophys. Res.*, *113*, D05202, doi:10.1029/2007JD009332.
- Cwiertny, D. M., R. M. Handler, M. V. Schaefer, V. H. Grassian, and M. M. Scherer (2008b), Interpreting nanoscale size-effects in aggregated Fe-oxide suspensions: Reaction of Fe(II) with Goethite, *Geochim. Cosmochim. Acta*, *72*, 1365–1380, doi:10.1016/j.gca.2007.12.018.
- Desboeufs, K. V., A. Sofikitis, R. Losno, J. L. Colin, and P. Aussel (2005), Dissolution and solubility of trace metals from natural and anthropogenic aerosol particulate matter, *Chemosphere*, *58*, 195–203, doi:10.1016/j.chemosphere.2004.02.025.
- Drake, N. A., A. S. El-Hawat, P. Turner, S. J. Armitage, M. J. Salem, K. H. White, and S. McLaren (2008), Palaeohydrology of the Fazzan Basin and surrounding regions: The last 7 million years, *Palaeogeogr. Palaeoclimatol. Palaeoecol.*, *263*, 131–145, doi:10.1016/j.palaeo.2008.02.005.
- Egli, M., P. Fitze, and A. Mirabella (2001), Weathering and evolution of soils formed on granitic, glacial deposits: Results from chronosequences of Swiss alpine environments, *Catena*, *45*, 19–47, doi:10.1016/S0341-8162(01)00138-2.
- Fan, S.-M., W. J. Moxim, and H. Levy II (2006), Aeolian input of bioavailable iron to the ocean, *Geophys. Res. Lett.*, *33*, L07602, doi:10.1029/2005GL024852.
- Fontes, M. R., S. B. Weed, and L. H. Bowen (1992), Association of microcrystalline goethite and humic acid in some oxisols from Brazil, *Soil Sci. Soc. Am. J.*, *56*, 982–990, doi:10.2136/sssaj1992.03615995005600030050x.
- Formenti, P., et al. (2008), Regional variability of the composition of mineral dust from western Africa: Results from the AMMA SOP0/DABEX and DODO field campaigns, *J. Geophys. Res.*, *113*, D00C13, doi:10.1029/2008JD009903.
- Fu, H., D. M. Cwiertny, G. R. Carmichael, M. M. Scherer, and V. H. Grassian (2010), Photoreductive dissolution of Fe-containing mineral dust particles in acidic media, *J. Geophys. Res.*, *115*, D11304, doi:10.1029/2009JD012702.

- Hand, J. L., N. M. Mahowald, Y. Chen, R. L. Siefert, C. Luo, A. Subramaniam, and I. Fung (2004), Estimates of atmospheric-processed soluble iron from observations and a global mineral aerosol model: Biogeochemical implications, *J. Geophys. Res.*, *109*, D17205, doi:10.1029/2004JD004574.
- Hegg, D. A., S. Gao, and H. Jonsson (2002), Measurements of selected dicarboxylic acids in marine cloud water, *Atmos. Res.*, *62*, 1–10, doi:10.1016/S0169-8095(02)00023-6.
- Hyacinthe, C., S. Bonneville, and P. Van Cappellen (2006), Reactive Iron (III) in sediments: Chemical versus microbial extractions, *Geochim. Cosmochim. Acta*, *70*, 4166–4180, doi:10.1016/j.gca.2006.05.018.
- Ita, A., and Y. Feng (2010), Role of dust alkalinity in acid mobilization of iron, *Atmos. Chem. Phys. Discuss.*, *10*, 10,399–10,428, doi:10.5194/acpd-10-10399-2010.
- Jickells, T. D., et al. (2005), Global iron connections between desert dust, ocean biogeochemistry, and Climate, *Science*, *308*, 67–71, doi:10.1126/science.1105959.
- Journet, E., K. V. Desboeufs, S. Caquineau, and J.-L. Colin (2008), Mineralogy as a critical factor of dust iron solubility, *Geophys. Res. Lett.*, *35*, L07805, doi:10.1029/2007GL031589.
- Kampf, N., and U. Schwertmann (1983), Goethite and hematite in a climosequence in southern Brazil and their application in classification of kaolinitic soils, *Geoderma*, *29*, 27–39, doi:10.1016/0016-7061(83)90028-9.
- Keene, W. C., A. A. P. Pszenny, J. R. Maben, and R. Sander (2002), Variation of marine aerosol acidity with particle size, *Geophys. Res. Lett.*, *29*(7), 1101, doi:10.1029/2001GL013881.
- Kostka, J. E., and G. W. Luther III (1994), Partitioning and speciation of solid phase iron in saltmarsh sediments, *Geochim. Cosmochim. Acta*, *58*, 1701–1710, doi:10.1016/0016-7037(94)90531-2.
- Lafon, S., J. L. Rajot, S. C. Alfaro, and A. Gaudichet (2004), Quantification of iron oxides in desert aerosol, *Atmos. Environ.*, *38*, 1211–1218, doi:10.1016/j.atmosenv.2003.11.006.
- Lafon, S., I. N. Sokolik, J. L. Rajot, S. Caquineau, and A. Gaudichet (2006), Characterization of iron oxides in mineral dust aerosols: Implications for light absorption, *J. Geophys. Res.*, *111*, D21207, doi:10.1029/2005JD007016.
- Lair, G. J., F. Zehetner, M. Hrachowitz, N. Franz, F. J. Maringer, and M. H. Gerzabek (2009), Dating of soil layers in a young floodplain using iron oxide crystallinity, *Quat. Geochronol.*, *4*, 260–266, doi:10.1016/j.quageo.2008.11.003.
- Lazaro, F. J., L. Gutierrez, V. Barron, and M. D. Gelado (2008), The speciation of iron in desert dust collected in Gran Canaria (Canary Islands): Combined chemical, magnetic and optical analysis, *Atmos. Environ.*, *42*, 8987–8996, doi:10.1016/j.atmosenv.2008.09.035.
- Leigh, D. S. (1996), Soil chronosequence of Brasstown Creek, Blue Ridge Mountains, USA, *Catena*, *26*, 99–114, doi:10.1016/0341-8162(95)00040-2.
- Luo, C., N. M. Mahowald, N. Meskhidze, Y. Chen, R. L. Siefert, A. R. Baker, and A. M. Johansen (2005), Estimation of iron solubility from observations and a global aerosol model, *J. Geophys. Res.*, *110*, D23307, doi:10.1029/2005JD006059.
- Mackie, D. S., P. W. Boyd, K. A. Hunter, and G. H. McTainsh (2005), Simulating the cloud processing of iron in Australian dust: PH and dust concentration, *Geophys. Res. Lett.*, *32*, L06809, doi:10.1029/2004GL022122.
- Mahowald, N. M., A. R. Baker, G. Bergametti, N. Brooks, R. A. Duce, T. D. Jickells, N. Kubilay, J. M. Prospero, and I. Tegen (2005), Atmospheric global dust cycle and iron inputs to the ocean, *Global Biogeochem. Cycles*, *19*, GB4025, doi:10.1029/2004GB002402.
- McFadden, I. D., and D. M. Hendricks (1985), Changes in the content and composition of pedogenic iron oxyhydroxides in a chronosequence of soils in southern California, *Quat. Res.*, *23*, 189–204, doi:10.1016/0033-5894(85)90028-6.
- McLennan, S. M. (1993), Weathering and global denudation, *J. Geol.*, *101*, 295–303, doi:10.1086/648222.
- Meskhidze, N., W. L. Chameides, A. Nenes, and G. Chen (2003), Iron mobilization in mineral dust: Can anthropogenic SO₂ emissions affect ocean productivity?, *Geophys. Res. Lett.*, *30*(21), 2085, doi:10.1029/2003GL018035.
- Meskhidze, N., W. L. Chameides, and A. Nenes (2005), Dust and pollution: A recipe for enhanced ocean fertilization?, *J. Geophys. Res.*, *110*, D03301, doi:10.1029/2004JD005082.
- Meunier, A., and B. Velde (2004), *Illite: Origins, Evolution, and Metamorphism*, Springer, Berlin.
- Mills, M. M., C. Ridame, M. Davey, J. La Roche, and R. J. Geider (2004), Iron and phosphorus co-limit nitrogen fixation in the eastern tropical North Atlantic, *Nature*, *429*, 292–294, doi:10.1038/nature02550.
- Moore, C. M., et al. (2009), Large-scale distribution of Atlantic nitrogen fixation controlled by iron availability, *Nat. Geosci.*, *2*, 867–871, doi:10.1038/ngeo667.
- Moreno, T., et al. (2006), Geochemical variations in Aeolian mineral particles from the Sahara-Sahel dust corridor, *Chemosphere*, *65*, 261–270, doi:10.1016/j.chemosphere.2006.02.052.
- Nesbitt, H. W., and G. M. Young (1982), Early Proterozoic climates and plate motions inferred from major element chemistry of lutites, *Nature*, *299*, 715–717, doi:10.1038/299715a0.
- Parker, A. (1970), An index of weathering for silicate rocks, *Geol. Mag.*, *107*, 501–504, doi:10.1017/S0016756800058581.
- Poulton, S. W., and D. E. Canfield (2005), Development of a sequential extraction procedure for iron: Implications for iron partitioning in continentally derived particulates, *Chem. Geol.*, *214*, 209–221, doi:10.1016/j.chemgeo.2004.09.003.
- Price, J. R., and M. A. Velbel (2003), Chemical weathering indices applied to weathering profiles developed on heterogeneous felsic metamorphic parent rocks, *Chem. Geol.*, *202*, 397–416, doi:10.1016/j.chemgeo.2002.11.001.
- Prospero, J. M., P. Ginoux, O. Torres, S. E. Nicholson, and T. E. Gill (2002), Environmental characterization of global sources of atmospheric soil dust dandified with the NIMBUS 7 Total Ozone Mapping Spectrometer (TOMS) absorbing aerosol product, *Rev. Geophys.*, *40*(1), 1002, doi:10.1029/2000RG000095.
- Pruppacher, H. R., and R. Jaenicke (1995), The processing of water vapor and aerosols by atmospheric clouds, a global estimate, *Atmos. Res.*, *38*, 283–295, doi:10.1016/0169-8095(94)00098-X.
- Raiswell, R., L. G. Benning, M. Tranter, and S. Tulaczyk (2008), Bioavailable iron in the Southern Ocean: The significance of the iceberg conveyor belt, *Geochem. Trans.*, *9*, 7, 9 pp., doi:10.1186/1467-4866-9-7.
- Reyes, I., and J. Torrent (1997), Citrate-ascorbate as a highly selective extractant for poorly crystalline iron oxides, *Soil Sci. Soc. Am. J.*, *61*, 1647–1654, doi:10.2136/sssaj1997.03615995006100060015x.
- Schroth, A. W., J. Crusius, E. R. Sholkovitz, and B. C. Bostick (2009), Iron solubility driven by speciation in dust sources to the ocean, *Nat. Geosci.*, *2*, 337–340, doi:10.1038/ngeo501.
- Schwertmann, U. (1991), Solubility and dissolution of iron oxides, *Plant Soil*, *130*, 1–25, doi:10.1007/BF00011851.
- Schwertmann, U., and M. Latham (1986), Properties of iron oxides in some New Caledonian soils, *Geoderma*, *39*, 105–123, doi:10.1016/0016-7061(86)90070-4.
- Shao, L., W. Li, Z. Xiao, and Z. Sun (2008), The mineralogy and possible sources of spring dust particles over Beijing, *Adv. Atmos. Sci.*, *25*, 395–403, doi:10.1007/s00376-008-0395-8.
- Shen, Z. X., J. J. Cao, X. Y. Zhang, R. Arimoto, J. F. Ji, W. L. Balsam, Y. Q. Wang, R. J. Zhang, and X. X. Li (2006), Spectroscopic analysis of iron-oxide minerals in aerosol particles from northern China, *Sci. Total Environ.*, *367*, 899–907, doi:10.1016/j.scitotenv.2006.01.003.
- Shi, Z., L. Shao, T. P. Jones, and S. Lu (2005), Microscopy and mineralogy of airborne particles collected during severe dust storm episodes in Beijing, China, *J. Geophys. Res.*, *110*, D01303, doi:10.1029/2004JD005073.
- Shi, Z., D. Zhang, M. Hayashi, H. Ogata, H. Ji, and W. Fujie (2008), Influences of sulfate and nitrate on the hygroscopic behaviors of coarse dust particles, *Atmos. Environ.*, *42*, 822–827, doi:10.1016/j.atmosenv.2007.10.037.
- Shi, Z., M. D. Krom, S. Bonneville, A. R. Baker, T. D. Jickells, and L. G. Benning (2009), Formation of iron nanoparticles and increase in iron reactivity in the mineral dust during simulated cloud processing, *Environ. Sci. Technol.*, *43*, 6592–6596, doi:10.1021/es901294g.
- Siefert, R. L., S. O. Pehkonen, Y. Erel, and M. R. Hoffmann (1994), Iron photochemistry of aqueous suspensions of ambient aerosol with added organic-acids, *Geochim. Cosmochim. Acta*, *58*(15), 3271–3279, doi:10.1016/0016-7037(94)90055-8.
- Solmon, F., P. Y. Chuang, N. Meskhidze, and Y. Chen (2009), Acidic processing of mineral dust iron by anthropogenic compounds over the North Pacific Ocean, *J. Geophys. Res.*, *114*, D02305, doi:10.1029/2008JD010417.
- Spokes, J. L., T. D. Jickells, and B. Lim (1994), Solubilisation of aerosol trace metals by cloud processing: A laboratory study, *Geochim. Cosmochim. Acta*, *58*, 3281–3287, doi:10.1016/0016-7037(94)90056-6.
- Straub, D. J., T. Lee, and J. L. Collett Jr. (2007), Chemical composition of marine stratocumulus clouds over the eastern Pacific Ocean, *J. Geophys. Res.*, *112*, D04307, doi:10.1029/2006JD007439.
- Sullivan, R. C., S. A. Guazzotti, D. A. Sodeman, and K. A. Prather (2007), Direct observations of the atmospheric processing of Asian mineral dust, *Atmos. Chem. Phys.*, *7*, 1213–1236, doi:10.5194/acp-7-1213-2007.
- Tegen, I., S. P. Harrison, K. Kohfeld, I. C. Prentice, M. Coe, and M. Heimann (2002), Impact of vegetation and preferential source areas

- on global dust aerosol: Results from a model study, *J. Geophys. Res.*, 107(D21), 4576, doi:10.1029/2001JD000963.
- Thompson, A., O. A. Chadwich, G. G. Rancourt, and J. Chorover (2006), Iron-oxide crystallinity increases during soil redox oscillations, *Geochim. Cosmochim. Acta*, 70, 1710–1727, doi:10.1016/j.gca.2005.12.005.
- Torrent, J., U. Schwertmann, and D. G. Schulze (1980), Iron oxide mineralogy of some soils of two river terrace sequences in Spain, *Geoderma*, 23, 191–208, doi:10.1016/0016-7061(80)90002-6.
- Torrent, J., Q. Liu, J. Bloemendal, and V. Barron (2007), Magnetic enhancement and iron oxides in the upper Luochuan loess-paleosol sequence, Chinese Loess plateau, *Soil Sci. Soc. Am. J.*, 71, 1570–1578, doi:10.2136/sssaj2006.0328.
- Uno, I., et al. (2009), Asian dust transported one full circuit around the globe, *Nat. Geosci.*, 2, 557–560, doi:10.1038/ngeo583.
- Varjo, E., A. Liikanen, V.-P. Salonen, and P. J. Martikainen (2003), A new gypsum-based technique to reduce methane and phosphorus release from sediments of eutrophied lakes: (Gypsum treatment to reduce internal loading), *Water Res.*, 37, 1–10, doi:10.1016/S0043-1354(02)00264-6.
- Viollier, E., P. W. Inglett, K. Hunter, A. N. Roychoudhury, and P. Van Cappellen (2000), The ferrozine method revisited: Fe(II)/Fe(III) determination in natural waters, *Appl. Geochem.*, 15, 785–790, doi:10.1016/S0883-2927(99)00097-9.
- Washington, R., C. Bouet, G. Cautenet, E. Mackenzie, I. Ashpole, S. Engelstaedter, G. Lizcano, G. M. Henerson, K. Schepanski, and I. Tegen (2009), Dust as a tipping element: The Bodélé Depression, Chad, *Proc. Natl. Acad. Sci.*, 106(49), 20,564–20,571, doi:10.1073/pnas.0711850106.
- Zhu, X., J. M. Prospero, F. J. Millero, D. L. Savoie, and G. W. Brass (1992), The solubility of ferric ion in marine mineral aerosol solutions at ambient relative humidities, *Mar. Chem.*, 38, 91–107, doi:10.1016/0304-4203(92)90069-M.
-
- A. R. Baker and T. Jickells, School of Environmental Sciences, University of East Anglia, Norwich NR4 7TJ, UK.
- L. G. Benning, S. Bonneville, M. D. Krom, and Z. Shi, Earth and Biosphere Institute, School of Earth and Environment, University of Leeds, Woodhouse Lane, Leeds LS2 9JT, UK. (shizongbo@163.com)
- C. Bristow, Department of Earth and Planetary Sciences, Birkbeck College, University of London, Malet Street, Bloomsbury, London WC1E 7HX, UK.
- K. Carslaw, G. Mann, and J. B. McQuaid, Institute of Climate and Atmospheric Sciences, School of Earth and Environment, University of Leeds, Maths/Earth and Environment Building, Leeds LS2 9JT, UK.
- N. Drake, Department of Geography, King's College London, Fourth Floor, Strand Campus, London WC2R 2LS, UK.